Emulation of quantum mechanical billiards by electrical resonance circuits

Olof Bengtsson, Johan Larsson, and Karl-Fredrik Berggren
Department of Physics and Measurement Technology, Linköping University, S-58183 Linköping, Sweden
(Received 31 March 2004; revised manuscript received 6 January 2005; published 13 May 2005)

We propose that a two-dimensional electric network may be used for fundamental studies of wave function properties, transport, and related statistics. Using Kirchhoff's current law and the $j\omega$ method we find that the network is analogous to a discretized Schrödinger equation for quantum billiards and dots. Thus complex electric potentials play the role of quantum mechanical wave functions. Ways of realizing the electric network are discussed briefly. The role of symmetries is outlined, and a direct way of selecting states with a given symmetry is presented.

DOI: 10.1103/PhysRevE.71.056206 PACS number(s): 05.45.Mt, 73.63.Kv, 84.30.−r, 89.20.−a

I. INTRODUCTION

Analogs to quantum mechanical (QM) billiards have proven useful for experimental studies of quantum chaos, wave function morphology, current statistics, vortex formation, and other topological issues. An advantage in going from the mesoscopic to macroscopic classical systems is that experimental conditions may be controlled precisely [1,2] and one may readily observe eigenfunctions, both their amplitude and phase, current, etc. For these reasons planar microwave cavities have been studied experimentally in, for example, Refs. [3–7]. The stationary Helmholtz equation for a perpendicular electric field E and wave number k

$$[\Delta + k^2]E = 0 \tag{1}$$

coincides with the time-independent Schrödinger equation for hard-walled quantum billiards [1]. Hence, micro- and matter waves in billiards are expected to behave in the same manner. There are also other classical wave analogs in for example acoustics, electromechanical systems, and surface waves in water vessels with arbitrary shape [1,2,8–10].

Here we propose another kind of emulation of quantum billiards based on electric networks. The idea behind this choice is the following. In numerical simulations of a quantum billiards one often relies on the finite difference method [11]. This implies that a computational grid (i,j) (row, column) is generated in the billiard, and an equation is formed at each such numerical grid point. Usually, only nearest neighbor interactions are considered. This implies that

$$\Delta f(x,y) \rightarrow \frac{f_{i+1,j} + f_{i-1,j} + f_{i,j+1} + f_{i,j-1} - 4f_{i,j}}{a^2} \tag{2}$$

giving the five-point approximation of the Schrödinger equation for QM billiards

$$-\frac{\hbar^2}{2ma^2}(\psi_{i,j-1} + \psi_{i-1,j} + \psi_{i,j+1} + \psi_{i+1,j} - 4\psi_{i,j}) = \mathcal{E}\psi_{i,j} \tag{3}$$

where $\psi_{i,j}$ is the value of the wave function at grid point (i,j), a the distance between nearest neighbors, m the particle mass, and $\mathcal{E}$ the energy eigenvalue. The discretized form in Eq. (3) now suggests that various types of lattice analogs to quantum billiards may be conceived. An obvious candidate is a mechanical system with springs and masses. However, Eq. (3) is also of the same form as the tight-binding model for a lattice of resonating monovalent atoms. We may therefore look for other discrete lattices constructed from identical objects with some characteristic oscillatory behavior. For example, an elementary, undamped electric circuit consisting of just a capacitor C and inductance L has the natural frequency $f_0 = 1/(2\pi\sqrt{LC})$. If N objects of this kind are brought together, the interactions between them will give rise to N collective oscillatory modes. We will therefore discuss how arrays of resonant electric circuits, constructed in close resemblance with the discretized Schrödinger equation in Eq. (3), represent interesting alternatives for emulating wave mechanics [12]. We will demonstrate that this type of systems offer rich possibilities for experimental studies of wave functions and, in particular, current morphology and statistics.

The idea about equivalent electric circuits to represent the Schrödinger equation is actually quite an old one, and was discussed by Kron [13] already in 1945. Later Manolache and Sandu [14] have investigated the eigenmodes of closed symmetric cavities. Statistical aspects are raised in the recent work by Bulgakov, Maksimov, and Sadreev [15]. This work and the present one are supplementary. Here we focus on wave function and current statistics and how symmetry may be probed by external ac voltage probes.

The paper is organized in the following way. In Sec. II we describe the design of equivalent *RLC* networks. Eigenmodes and resonant features are discussed in Sec. III for open and closed "electric billiards." The relation between the quantum mechanical probability current and its network analog is outlined in Sec. IV. In Sec. V we propose a way to disentangle different symmetry states in billards with external driving voltages. Section VI focuses on statistics and, finally, Sec. VII contains a discussion and concluding remarks.

II. AN ELECTRIC NETWORK ANALOG

An electrical grid is designed according to Fig. 1. The grid consists of capacitances C, inductances L, and resistances R. Here, we focus on a grid shaped geometrically as in Fig. 2. This is the same shape as used in the microwave studies in Refs. [3–6], originally chosen for studies of wave

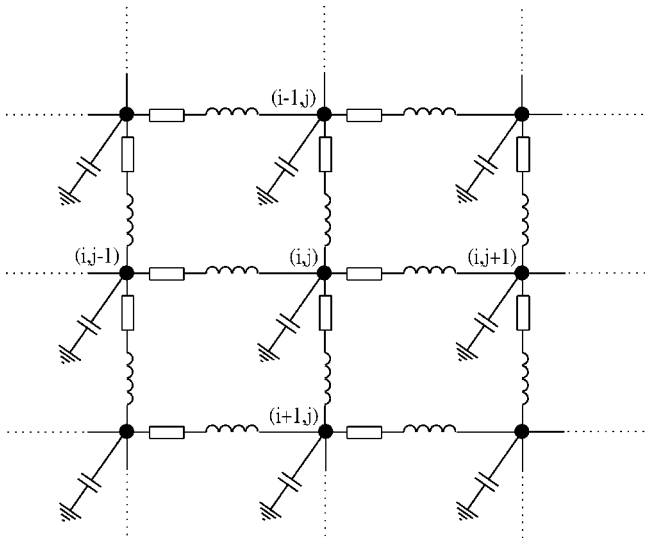

FIG. 1. Internal points in a grid.

function scarring in a quantum dot with two leads [16]. Consequently there is experimental work for comparison. There are also quantum mechanical computations [17] for the same kind of billiard in which source and drain are emulated by small imaginary potentials $\pm i\Gamma$ in the regions of the two leads. Because of the shape of the cavity, effectively an open half stadium, we will recover regular as well as irregular modes. To disentangle symmetries we will also consider an entire stadium with up to four external driving voltages.

As above, all grid points in Fig. 2 are grounded via a capacitor and connected to its neighboring grid points through an inductance in series with a resistance. The resistances are important for a more realistic modeling of the coils used in the practical case. Other phenomena, such as leakage and resistance in the capacitances, can also easily be added as a parallel and/or a serial resistance to the capacitances if desired. Leakage in billiards may be simulated by selecting adequate values for the resistances.

To probe the dynamics of the networked billiard one or multiple grid points are selected, to which an alternating sinusoidal voltage in series with a load resistance is attached as in Fig. 3. The inward current through this resistance as a function of the angular frequency ω will later prove useful. Using the $j\omega$ method and Kirchhoff's current law [18], i.e.,

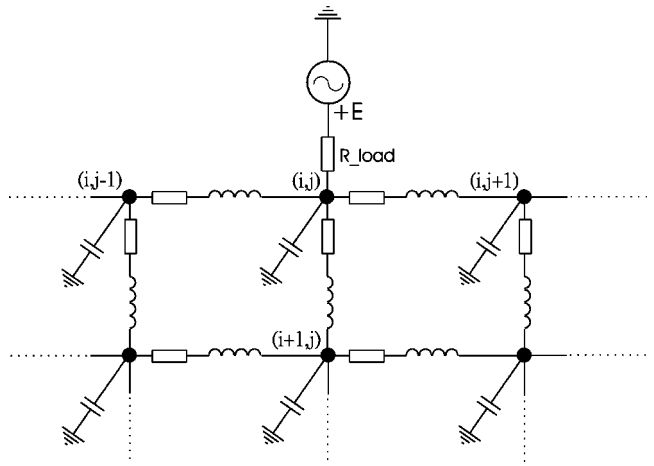

FIG. 3. Grid with connected voltage.

the sum of all currents into a node p equals zero, equations of the form

$$\sum_k I_{k,p} = \sum_k \frac{V_k - V_p}{Z_{kp}} = 0 \tag{4}$$

are obtained; k runs over all directions from node p in which a current can flow, and Z_{kp} is the impedance between the potentials V_k and V_p.

For a typical internal point, where i gives the vertical and j the horizontal position, the pair (i,j) gives the location of the point in the grid (see Fig. 1). By using the notation $Z_l = R + j\omega L$ and $Z_c = 1/j\omega C$, where $j = \sqrt{-1}$, L the inductance, C the capacitance, and R the resistance of the components in question, equations of the form

$$\frac{V_{i,j-1} - V_{i,j}}{Z_l} + \frac{V_{i-1,j} - V_{i,j}}{Z_l} + \frac{V_{i,j+1} - V_{i,j}}{Z_l} + \frac{V_{i+1,j} - V_{i,j}}{Z_l} + \frac{0 - V_{i,j}}{Z_c} = 0 \tag{5}$$

are generated. This equation may be rewritten as

$$-(V_{i,j-1} + V_{i-1,j} + V_{i,j+1} + V_{i+1,j} - 4V_{i,j}) = -\frac{Z_l}{Z_c} V_{i,j}, \tag{6}$$

which clearly is of the same form as Eq. (3).

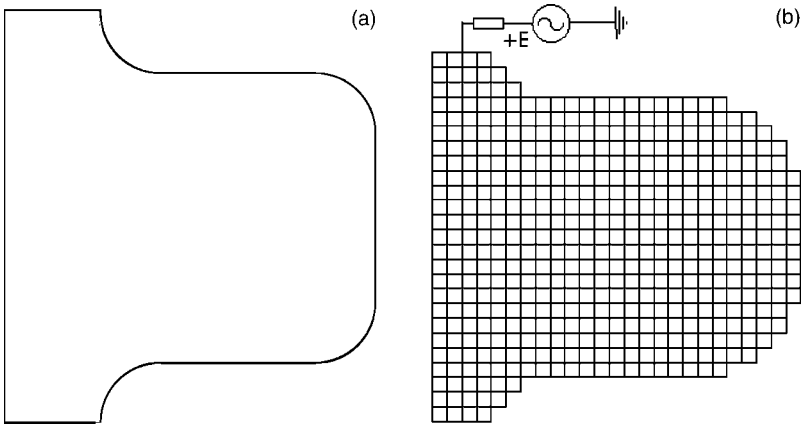

FIG. 2. Modeling of a "two-lead" cavity in the shape of an open quantum dot.

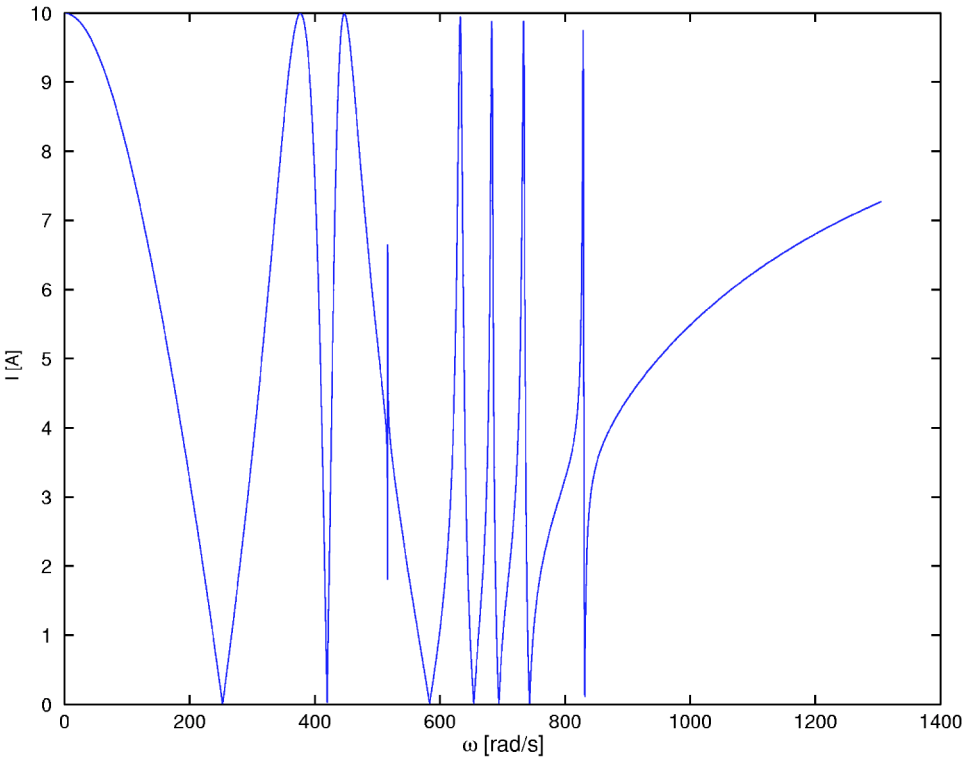

FIG. 4. (Color online) A typical plot of the current $|I|$ as a function of ω for a small net. Each minimum is an eigenfrequency.

For a node connected to a source instead of having a neighboring node at $(i-1,j)$ as in Fig. 3, we get

$$\frac{V_{i,j-1}-V_{i,j}}{Z_l}+\frac{(0+E)-V_{i,j}}{R_{\text{load}}}+\frac{V_{i,j+1}-V_{i,j}}{Z_l}+\frac{V_{i+1,j}-V_{i,j}}{Z_l}+\frac{0-V_{i,j}}{Z_c}=0 \tag{7}$$

where E is the amplitude of the driving voltage.

The size of the grid determines the resolution of the wave mechanical state we wish to emulate and is comparable to digital sampling of a propagating wave. This means that higher frequencies require a larger grid to get the desired resolution, but also that effects of sampling, such as alias distortion, might occur [18].

Below we will see that one may identify the quantum mechanical wave function ψ with the potential field V, and that the energy $\mathcal{E}$ of the quantum mechanical system corresponds to the squared angular frequency ω^2.

III. NETWORK EIGENMODES AND RESONANCES

Here, two ways of finding the modes of the networked billiard are presented, i.e., for an "open" billiard with external driving voltages and for a "closed" one without them.

In open microwave cavities the characteristic modes are found as peaks when studying the transmission through the system as a function of frequency [1]. A similar plot may be produced by studying the current

$$I=\frac{E-V_{i,j}}{R_{\text{load}}} \tag{8}$$

through R_{load} as a function of the angular frequency. It turns out that resonant eigenmodes are found at the minima of this curve. The current reaches its upper value at low and high frequencies, which is related to the characteristic performance of the components. An inductance behaves as a short circuit at low frequencies, while a capacitance acts as a short circuit at high frequencies. This means that the system is only active in the middle region, resulting in a maximum current $I_{\text{max}}=E/R_{\text{load}}$ as seen in Fig. 4 at both ends of the spectrum.

In the second approach, eigenvalues are extracted in the same way as for a closed quantum billiard. For this purpose all equations for $V_{i,j}$ must be cast in the same form, and Dirichlet boundary conditions should be implemented in a

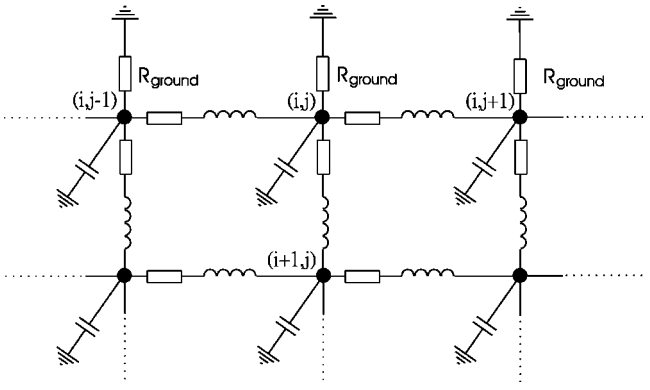

FIG. 5. Grid with alternative boundary conditions.

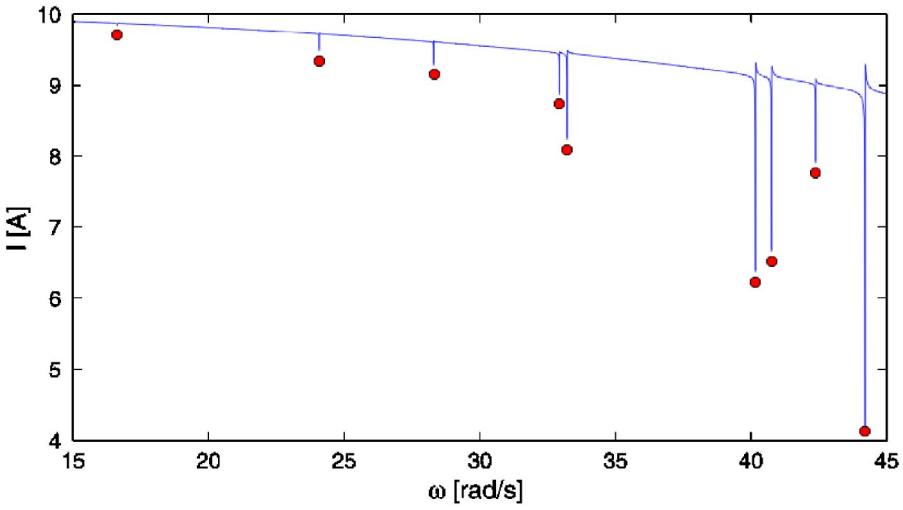

FIG. 6. (Color online) Current $|I|$ through the load resistance, with marked dips for a selected ω region.

slightly different manner. Hence we insert a very small resistance R_{ground} between the grid point and ground as in Fig. 5. The equation for a grounded point (i,j) in Fig. 5 is then

$$-\left[V_{i,j-1}+V_{i,j+1}+V_{i+1,j}-\left(3+\frac{1}{R_{\text{ground}}}\right)V_{i,j}\right]=-\frac{Z_l}{Z_c}V_{i,j}. \tag{9}$$

By handling the Dirichlet boundary conditions in this way the system may be written as an eigenvalue equation

$$\mathbb{B}\mathbf{V}=-\frac{Z_l}{Z_c}\mathbf{V} \tag{10}$$

where $\mathbb{B}$ is a matrix corresponding to the Hamiltonian H in a quantum mechanical system. By assuming that R is small and may be neglected we have $Z_l/Z_c \approx -\omega^2 LC$. Hence solutions $\mathbf{V}$ are real and

$$\omega=\sqrt{\frac{\text{eig}(\mathbb{B})}{LC}} \tag{11}$$

gives the angular frequencies for the collective eigenstates.

There should, however, be some differences between modes found from the two separate methods, i.e., with and without an external driving voltage. When comparing the values for $|V_{i,j}|^2$, generated by the two different methods one can hardly see any difference in the cases investigated here. The actual voltages differ, though. By studying, for example, the analog to the quantum mechanical probability current, which is treated below, differences in phase are observed. Therefore the latter method is suitable for generating images of eigenmodes, or for finding the angular frequencies at which they occur.

In Fig. 6 we show the current through the load resistance and how the resonant modes may be identified as narrow dips as outlined above. The computations were based on the device parameters $L=10$ mH, $C=1$ mF, $R=0.05$ mΩ, $R_{\text{load}}=1$ Ω, and $E=10$ V, values which are also assumed throughout the remaining part of our presentation. These values are

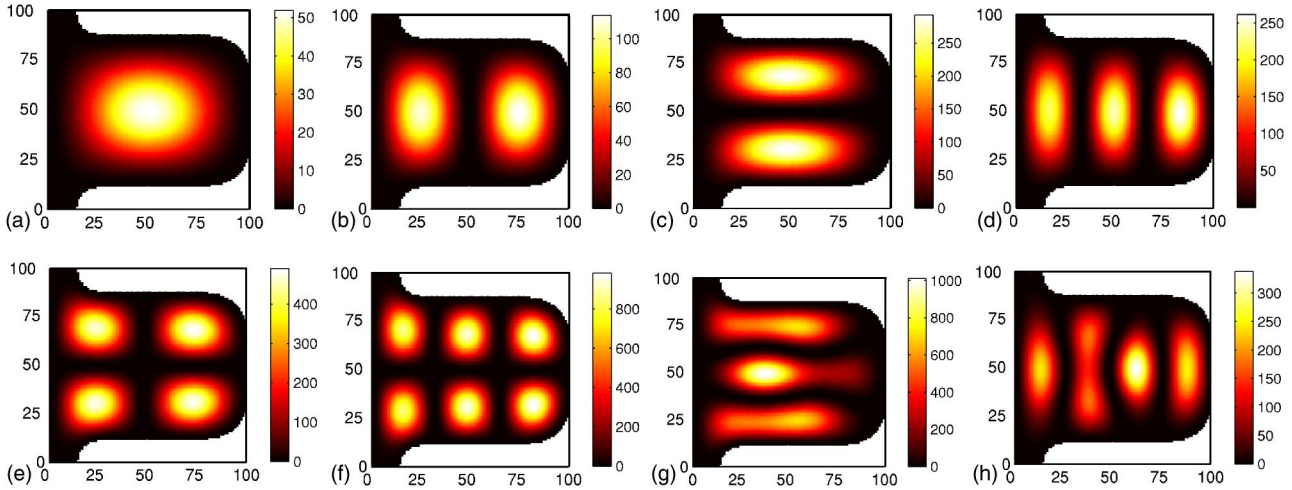

FIG. 7. (Color online) The first eight modes, showing $|V|^2$, to be compared with $|\psi|^2$ in QM. The number of grid points (i,j) is 100 $\times$100, and the values $L=10$ mH, $C=1$ mF, and $R=0.05$ mΩ were used in the simulations.

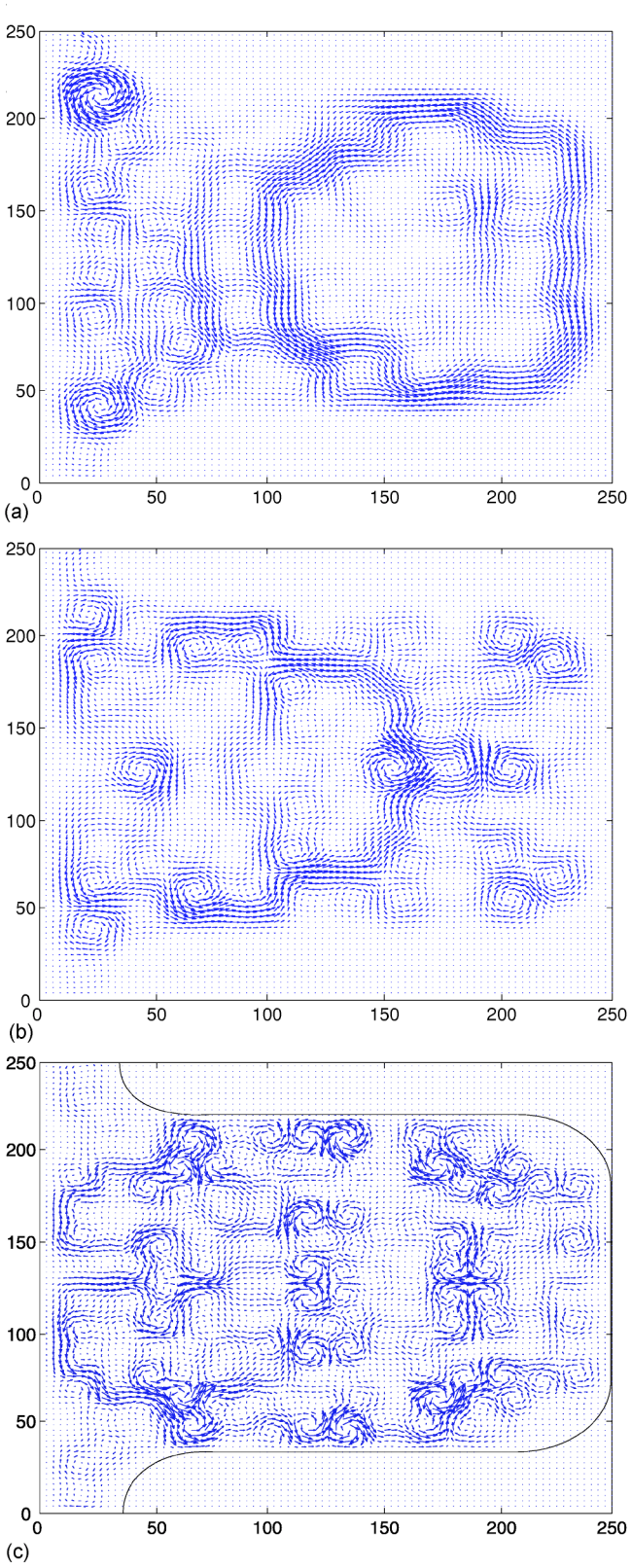

FIG. 8. (Color online) Poynting vector fields, corresponding to modes 67, 75, and 175. Grid points indices (i,j) are indicated on the horizontal and vertical axes (cf. Figs. 1 and 2).

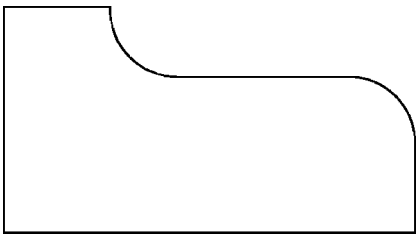

FIG. 9. A desymmetrized two-lead cavity, isolating the *odd* wave functions.

not standard device parameters. However, this is of less concern here since it is really the ratio between them that matters. The first eight resonant modes, starting with the mode corresponding to the lowest energy, can be seen in Fig. 7. Comparisons with microwave measurements [3,5] and quantum mechanical calculations [17] verify that $|V|^2$ indeed mimics $|\psi|^2$ in a very satisfactory way.

IV. CURRENTS

To investigate further the correspondence between ψ and V we study the transmission through the system. An analog to the QM probability current

$$\mathbf{j} = \frac{\hbar}{m}\mathrm{Im}\{\psi^* \nabla \psi\} \tag{12}$$

is obtained by replacing the wave function ψ with our potential field V. Hence, omitting constants we have

$$\mathbf{S} = \mathrm{Im}\{V^* \nabla V\} \tag{13}$$

which is, in fact, a Poynting vector for our system. With

$$\frac{\partial}{\partial x}V(i,j) \propto (V_{i,j+1} - V_{i,j-1}) \tag{14}$$

we obtain a Poynting vector, which in our system is given by

$$\mathbf{S} \approx \mathrm{Im}\begin{pmatrix} V_{i,j}^*(V_{i,j+1} - V_{i,j-1}) \\ V_{i,j}^*(V_{i-1,j} - V_{i+1,j}) \end{pmatrix}. \tag{15}$$

Another, more intuitive way of obtaining **S** is to study the complex electrical effect S_c given by $S_c = UI^*$, and especially $P = \mathrm{Re}\{S_c\}$, which is the measured electrical effect. Assigning to P the direction of the current gives a vector

$$\mathbf{P} = \mathrm{Re}\begin{pmatrix} V_{i,j}\left(\frac{V_{i,j+1}-V_{i,j-1}}{2Z_l}\right)^* \\ V_{i,j}\left(\frac{V_{i-1,j}-V_{i+1,j}}{2Z_l}\right)^* \end{pmatrix} = \mathrm{Re}\begin{pmatrix} V_{i,j}\left(\frac{V_{i,j+1}-V_{i,j-1}}{2(j\omega L+R)}\right)^* \\ V_{i,j}\left(\frac{V_{i-1,j}-V_{i+1,j}}{2(j\omega L+R)}\right)^* \end{pmatrix}. \tag{16}$$

By realizing that R is small and therefore negligible, and suppressing the factor $2\omega L$ in the denominator, we get

$$\tilde{\mathbf{P}} = \mathrm{Re}\begin{pmatrix} V_{i,j}\left(\frac{V_{i,j+1}-V_{i,j-1}}{j}\right)^* \\ V_{i,j}\left(\frac{V_{i-1,j}-V_{i+1,j}}{j}\right)^* \end{pmatrix} = \mathrm{Im}\begin{pmatrix} V_{i,j}^*(V_{i,j+1} - V_{i,j-1}) \\ V_{i,j}^*(V_{i-1,j} - V_{i+1,j}) \end{pmatrix} \tag{17}$$

which is equal to **S**.

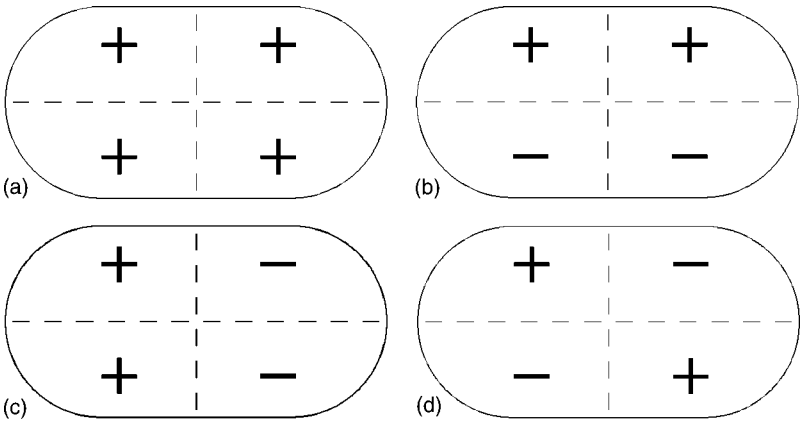

FIG. 10. Symmetries in the Bunimovich billiard.

To illustrate the current distribution we show the case with only one external driving voltage in the grid as in Fig. 2(b) and save the multilead case for the next section. Of course, with only one external voltage present we break the symmetry. As the frequency increases the lack of symmetry becomes, however, less and less prominent. Plots showing flow patterns analogous to the quantum mechanical probability current are displayed in Fig. 8. Similarities with the results of microwave measurements [5] and quantum mechanical calculations [17] are most striking.

V. EXTRACTION OF SYMMETRIES

Identification of modes belonging to a certain symmetry class in a billiard is often required. An example is statistics, which many times refer to a particular symmetry class. As discussed above, we have two ways of finding the characteristic modes. Consequently there are also two ways of selecting the modes belonging to a particular symmetry class.

In the case of level statistics, the eigenvalue approach, Eqs. (10) and (11) in Sec. III, appears a convenient one from a computational point of view, since many modes are found in a relatively short time. Extraction of, for example, odd modes is done here by "desymmetrizing" the billiard. Dirichlet boundary conditions are achieved by grounding the billiard along the middle symmetry line, and then by studying only one-half of the billiard. The desymmetrized billiard is shown in Fig. 9.

Let us now turn to the other way of finding characteristic modes by driving the system by external voltages. This approach is, of course, more realistic when it comes to practical measurements. It also appears quite elegant. To make the case a bit more general we now consider a network in the shape of a full Bunimovich billiard (Fig. 10). The two lines of symmetry run along the middle of the billiard, one in the horizontal and one in the vertical direction, dividing the Bunimovich billiard into four parts; top left, top right, bottom left, and bottom right. By marking each section with either a "+" or a "−," we may specify the different symmetries. If the same sign occurs on each side of a symmetry line, the wave function is *even*, with respect to this line. On the other hand, if the signs are different, the wave equation is odd. The possibilities can be referred to as even/even, even/odd, odd/even, and odd/odd (referring to the horizontal/vertical direction).

The four different symmetry classes in Fig. 10 are generated by connecting a voltage to each of the four sections as in Fig. 11. The external voltages must be connected symmetrically, if the desired symmetry class is to be selected. The phase of the driving voltages is then used to achieve symmetry or antisymmetry, with respect to the symmetry lines. One way to view this is by studying the modes given by each voltage separately, and then add them together by means of superposition. In this way one understands why some modes are canceled and others not. For example, if one drives equal currents into the billiard on each side of a line of symmetry, modes with a node on the symmetry line will disappear. At the same time, even wave functions are amplified.

Thus, we can define a "+" by connecting a voltage driving a current into the billiard, and a "−" by connecting a voltage driving a current out of the billiard at a given time $t=0$. The situation in Fig. 10(d), isolating the odd/odd wave functions, is realized with the network in Fig. 11. We have verified our approach by explicit numerical calculations. In doing so we have found that it is important that the external voltages are placed and driven symmetrically with high precision. For example, displacing one or more of them gives rise to a superposition of symmetry classes.

In the same way as proposed here, it should also be possible to extract states with a particular symmetry for cases like microwave cavities, elastic membranes, and acoustic resonators.

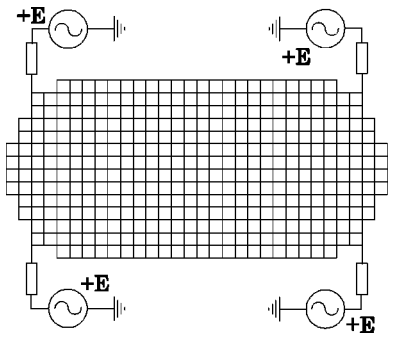

FIG. 11. A stadium shaped grid giving the odd/odd symmetry class. The four different positions of the symbol *E* with respect to the voltage sources define the phases, in our case equal or opposite.

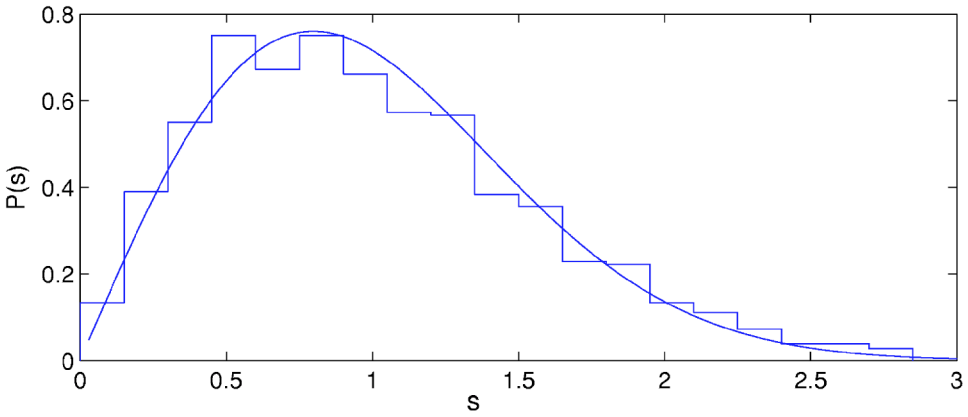

FIG. 12. (Color online) Statistics for the normalized angular frequency spacings ω^2, corresponding to the spacings between eigenenergies in quantum mechanics. The curve is the Wigner-Dyson distribution given by Eq. (19); 1199 spacings for the half billiard in Fig. 9 were used for generating the histogram.

VI. STATISTICAL PROPERTIES

Statistical aspects are important signatures of quantum mechanical systems. In order to validate the present electric network model we will compare its statistical predictions with the quantum case. Focus lies on the spacings between eigenenergies, distributions of wave function amplitudes and intensities, and statistics for the quantum mechanical probability current. Ideally our network system should follow the same statistics as the QM system we intend to emulate. All statistics presented below refer to the billiard in Fig. 2, without and with external driving voltages, i.e., "closed" or "open."

For a classically integrable, i.e., nonchaotic, QM system with time reversal symmetry (TRS) one expects the Poisson distribution given by [1,2]

$$P(s) = e^{-s} \tag{18}$$

for the distribution of normalized spacings s between eigenenergies. On the other hand, for an irregular chaotic system with TRS one finds generally the Wigner-Dyson distribution

$$P(s) = \frac{s\pi}{2}\exp(-\pi s^2/4). \tag{19}$$

As mentioned, in our case ω^2 corresponds to the QM energy $\mathcal{E}$. Figure 12 shows the distribution of normalized level separations for odd states, i.e., states in the half cavity without external driving voltages as in Fig. 9. Real values for ω^2 are computed from Eqs. (10) and (11) in Sec. III. As mentioned previously

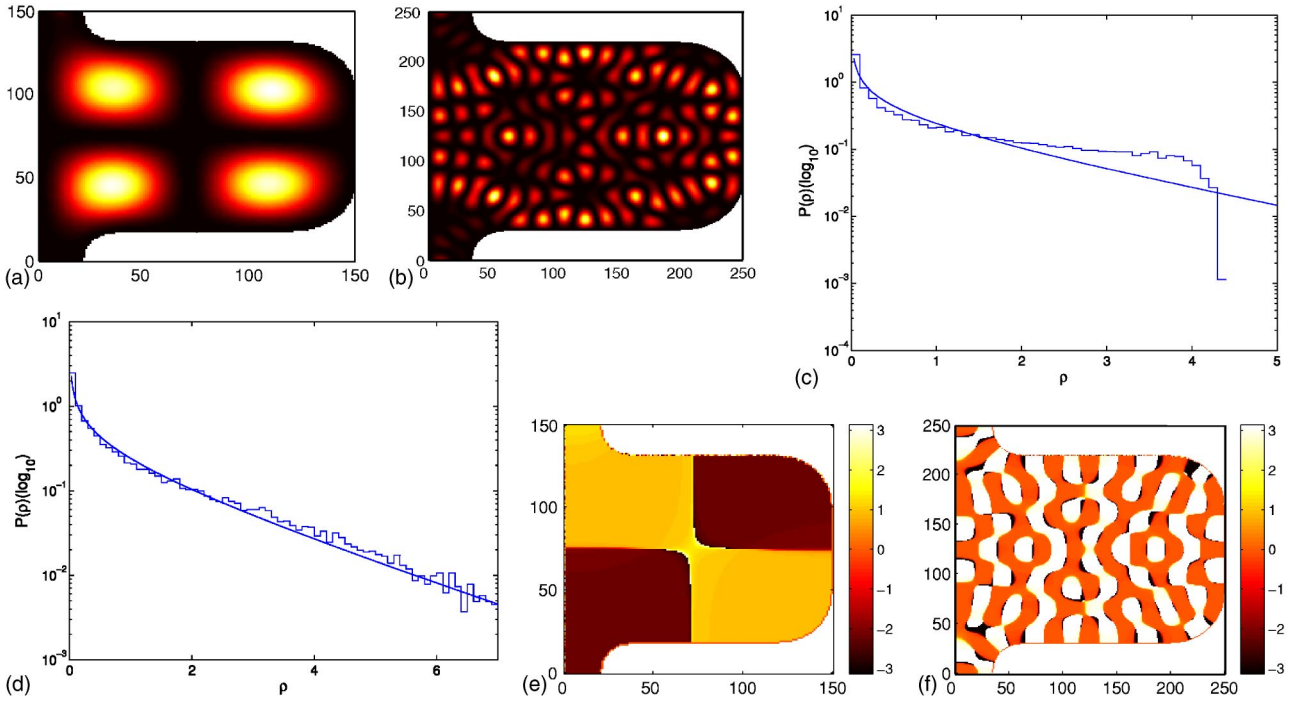

FIG. 13. (Color online) (a) shows $|V_{i,j}|^2$ for a regular resonant eigenmode and (b) for a chaotic resonant mode. The curve in (c) and (d) is the Porter-Thomas distribution in Eq. (20) for (a) and (b), respectively. (e) and (f) show the phase of the "wave function" $V_{i,j}$ for (a) and (b). The behavior of the statistics in (c), i.e., the way the tail suddenly drops to zero, is a general characteristic for regular modes [10,20]. The number of grid points is indicated on the horizontal and vertical axes.

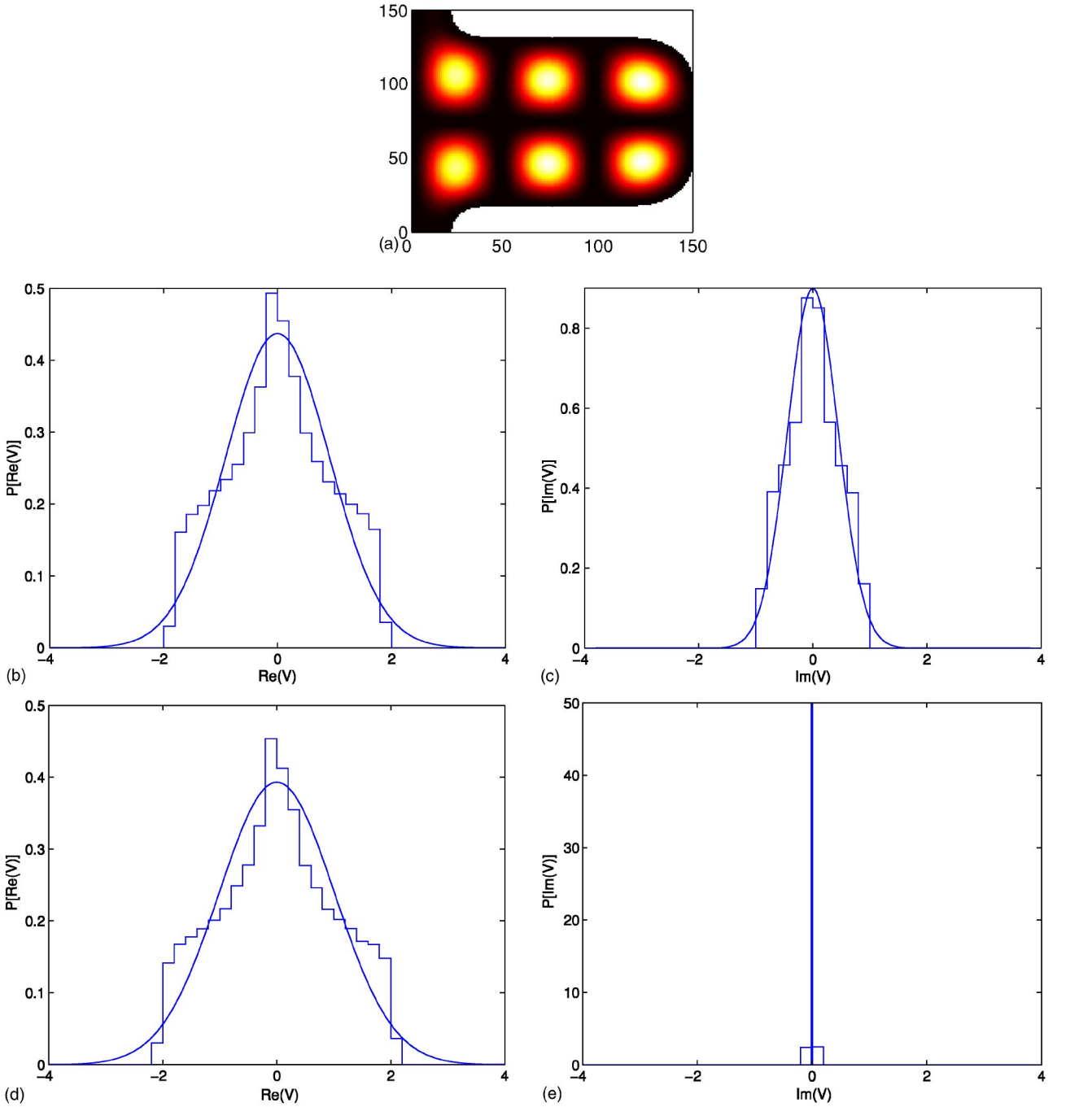

FIG. 14. (Color online) (a) shows $|V_{i,j}|^2$ for a regular state with $\omega=26.65$ rad/s, and (b)–(e) the distributions for the real and imaginary parts of the potential field $V_{i,j}$, before and after a rotation by the angle α, defined by Eq. (24). The curves are Gaussian distributions, Eq. (23), with parameters given in each subfigure. The number of grid points is indicated on the horizontal and vertical axes.

there are both regular and irregular solutions for the systems at hand. The good agreement between the computed distribution and the Wigner-Dyson expression tells us, however, that the states are almost exclusively chaotic with TRS.

In quantum mechanics wave function statistics for the different modes are of obvious interest. For a billiard with area A a distribution $P(\rho)$ may be produced, where $\rho=A|\psi|^2$, giving the probability of finding a certain intensity $|\psi|^2$. $P(\rho)$ follows the well known Porter-Thomas distribution [1,2]

$$P(\rho) = \frac{1}{\sqrt{2\pi\rho}} e^{-\rho/2} \tag{20}$$

for systems with TRS. For broken TRS the Thomas-Porter form is replaced by the exponential Rayleigh distribution

$$P(\rho) = e^{-\rho}. \tag{21}$$

There is also the case of intermediate statistics as discussed in [19,20] and references within. Figure 13 shows statistics

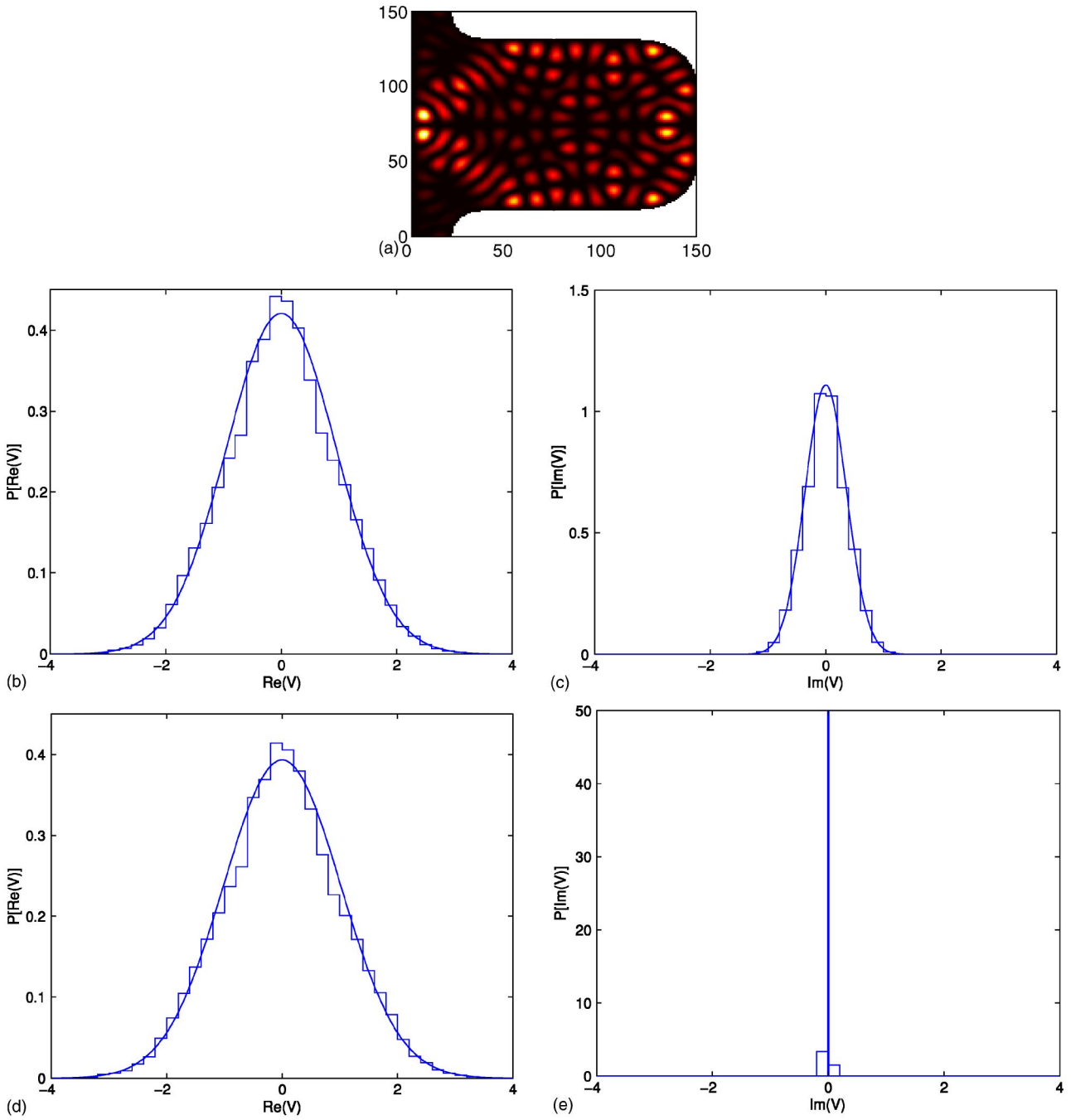

FIG. 15. (Color online) (a) shows $|V_{i,j}|^2$ for an irregular state with $\omega = 112.41$ rad/s, and (b)–(e) the corresponding distributions for the real and imaginary parts of the potential field $V_{i,j}$, before and after a rotation by the angle α, given by Eq. (24). The curves are Gaussian distributions, Eq. (23), with parameters given in each subfigure. The number of grid points are indicated on the horizontal and vertical axes.

for two resonant modes for an open system, at low and high frequencies, respectively. The high-frequency mode obviously obeys the Thomas-Porter distribution to a high degree of accuracy. In view of the level statistics above chaotic behavior is to be expected. The low-frequency mode, on the other hand, is an example of a regular mode and for this reason it displays a characteristic dropoff behavior at high intensities [10,20].

The solutions for the open billiard are complex and TRS is, in principle, broken. In spite of this, the Thomas-Porter distribution applies to a high degree of accuracy to the irregular states, for example. To analyze this situation it is useful to consider the general complex wave function [19,20]

$$\psi = u + iv \tag{22}$$

where u is the real and and v the imaginary part, which for chaotic states are treated as two independent Gaussian fields. For later reference denote the Gaussian distribution as

$$P(s) = \frac{1}{\sigma\sqrt{2\pi}} e^{-(s-\mu)/2\sigma^2} \tag{23}$$

where σ is the standard deviation and μ the center value.

Intuitively the relative weights of u and v indicate which kind of statistics a particular state obeys. If either u or v is the dominant term, for example, we expect the Thomas-Porter distribution for an irregular state. On the hand, if u and v have more or less equal weights we expect the Rayleigh distribution or an intermediate crossover form. To make this statement valid we must, however, make sure that the real and imaginary parts in the wave function are statistically independent as discussed in [19,20]. This is achieved by multiplying the wave function by the phase factor $e^{i\alpha}$. By letting $\langle \cdots \rangle$ indicate the mean value, α can be written as

$$\alpha = \frac{1}{2}\arctan\left(\frac{2\langle uv\rangle}{\langle u\rangle^2 - \langle v\rangle^2}\right), \tag{24}$$

giving a rotation of all points by the angle α in the complex plane. This rotation is in fact derived from the expression $\langle uv\rangle = 0$, thus ensuring that the fields are also uncorrelated. Note that one may instead make the imaginary part dominant by adding one more rotation with an odd multiple of $\pi/2$. As indicated already, the Rayleigh distribution instead emerges when the real and the imaginary parts of the wave function are of equal magnitude. Hence, neither of the two fields can be made dominant over the other, and the rotation above only makes the fields statistically independent.

The fact that the statistics for both real and imaginary parts of the amplitudes follow a Gaussian distribution has been verified for numerous resonant modes. Figures 14 and 15 show distributions for the real and imaginary parts of the amplitudes for two typical modes, both before and after the rotation given by Eq. (24). Obviously the real part dominates by far over the imaginary one after the rotation. This explains why the resonant modes obey distributions typical for TRS like the Thomas-Porter distribution. In our computations we have found that the phase appears to change continuously, but as soon as a resonant eigenmode appears, the wave pattern is close to real, i.e., the phase of the amplitude in each point is close to zero or π.

Finally we consider the quantum mechanical probability current for an open system, which also follows certain universal statistics for irregular states [19,21,22]. Regular states are discussed in Ref. [23]. One may either study the components or the absolute value of the current $\mathbf{j}$. If the net current is small the components should obey

$$P(j_d) = \frac{1}{2\tau} e^{-|j_d|/\tau} \tag{25}$$

for chaotic states (d indicates the horizontal or the vertical direction). At the same time, the absolute value follows the universal law

$$P(|\mathbf{j}|) = \frac{|\mathbf{j}|}{\tau^2} K_0\left(\frac{|\mathbf{j}|}{\tau}\right) \tag{26}$$

where K_0 is the modified Bessel function of the second kind, zeroth order, and τ is a function depending on the standard deviation of the wave function. The value of τ may be computed from the solution $V_{i,j}$, but here τ will be treated as a fitting parameter, used merely to see if the statistics follow the generic form predicted by the theory.

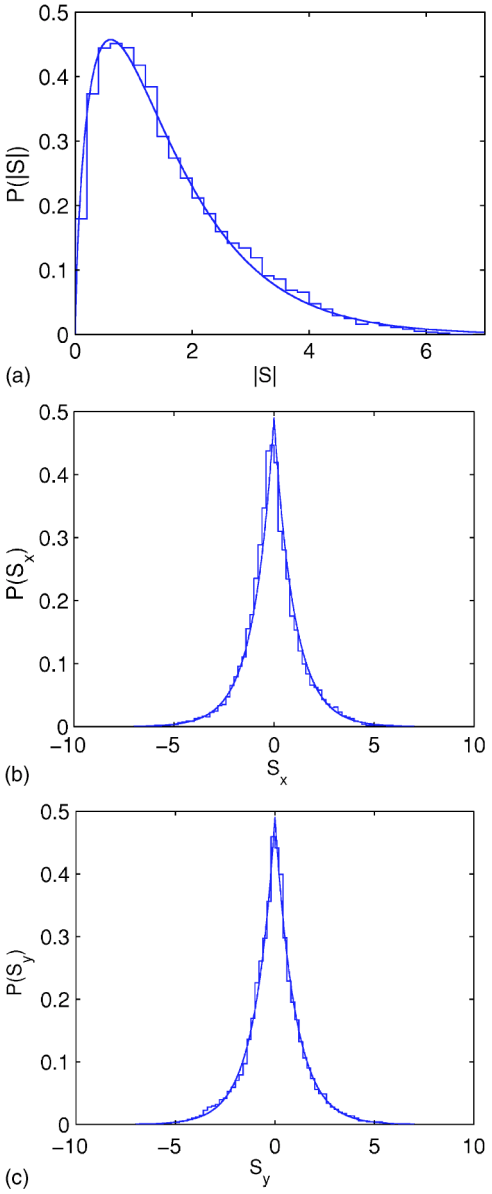

FIG. 16. (Color online) Statistics for a typical high-frequency mode. The curve in (b) is given by Eq. (26), and the curves in (c) and (d) by Eq. (25). The fitting parameter is $\tau = 2.0$.

Figure 16 shows histograms for distributions for a typical chaotic high-frequency resonant mode with ψ replaced by V and $\mathbf{j}$ by $\mathbf{S}$. The numerical results for our electric network obviously agree nicely with theoretical predictions for random fields.

VII. DISCUSSION AND CONCLUDING REMARKS

In summary, we have proposed that electrical networks may be used for fundamental studies of wave function properties and transport in general and, more specifically, their

mapping onto open quantum dots. By connecting each grid point to some light source, as for example light-emitting diodes, the wave patterns might be observed in real time. The role of dissipation and breaking of TRS may also be studied in a controlled way via the resistances. One could also model any billiard; it is only a question of grounding certain grid points. In addition to the scientific case our network has obvious pedagogical merits.

There are two ways (at least) for physically realizing our net. A first straightforward one is to use passive components (as in Fig. 1). Ideally the components should all be identical but for practical purposes we have made simulations with randomized values (±10%) for the components. The grid was still functional in this case. The demands on the performance of components are, however, high. Standard components have problems in working over large frequency intervals as their performance deteriorates at higher frequencies. One may circumvent this problem by working with large networks in which the eigenstates are more close packed. Superconducting materials may then be useful to reduce R and dissipation.

A second way to realize our electric simulator is by using active components, such as operational amplifiers [18], to mimic the behavior of the ordinary components. This second alternative is the one we believe to be more promising.

ACKNOWLEDGMENTS

We acknowledge discussions with Almas Sadreev, in particular in the initial phase of this project, with Jani Hakanen about computational issues and comparisons to his quantum mechanical calculations, and Lars Wanhammar about electric circuits.

[1] H.-J. Stckmann, *Quantum Chaos: An Introduction* (Cambridge University Press, Cambridge, U.K., 1999).
[2] T. Guhr, A. Müller-Groeling, and H. A. Weidenmüller, Phys. Rep. **299**, 189 (1998), and references within.
[3] Y.-H. Kim, M. Barth, H.-J Stöckmann, and J. P. Bird, Phys. Rev. B **65**, 165317 (2002).
[4] M. Barth and H.-J Stöckmann, Phys. Rev. E **65**, 066208 (2002).
[5] M. Barth, Ph.D. dissertation, Philipps-Universität, Marburg, 2001.
[6] Y.-H. Kim, M. Barth, U. Kuhl, and H. J Stöckmann, Prog. Theor. Phys. Suppl. **150**, 105 (2003).
[7] C. Dembrowski, H.-D. Gräf, H. L. Harney, A. Heine, W. D. Heiss, H. Rehfeld, and A. Richter, Phys. Rev. Lett. **86**, 787 (2001).
[8] J. D. Maynard, Rev. Mod. Phys. **73**, 401 (2001).
[9] K. Schaadt, T. Guhr, C. Ellegaard, and M. Oxborrow, Phys. Rev. E **68**, 036205 (2003).
[10] K. Schaadt, Ph.D. dissertation, Niels Bohr Institute, University of Copenhagen, 2001.
[11] F. J. Vesely, *Computational Physics: An Introduction* (Plenum Press, New York, 1994).
[12] For a preliminary discussion about the mapping of the discretized Schrödinger equation for closed billiards onto *RLC* networks, see K.-F. Berggren and A. F. Sadreev, in *Proceedings of the Conference on Mathematical Modelling of Wave Phenomena, 2002*, edited by B. Nilsson and L. Fishman, Mathematical Modelling in Physics, Engineering and Cognitive Sciences Vol. 7 (Växjö University Press, Växjö, 2004).
[13] G. Kron, Phys. Rev. **67**, 39 (1945).
[14] F. Manolache and D. D. Sandu, Phys. Rev. A **49**, 2318 (1994).
[15] E. N. Bulgakov, D. N. Maksimov, and A. F. Sadreev, Phys. Rev. E **71**, 046205 (2005).
[16] J. P. Bird, R. Akis, D. K. Ferry, A. P. S de Moura, Y.-C. Lai, and K. M. Indlekofer, Rep. Prog. Phys. **66**, 583 (2003).
[17] K.-F. Berggren, I. I. Yakimenko, and J. Hakanen (unpublished).
[18] C. R. Paul, S. A. Nasar, and L. E. Unnewahr, *Introduction to Electrical Engineering* (McGraw-Hill, Singapore, 1992).
[19] A. I. Saichev, H. Ishio, A. F. Sadreev, and K.-F. Berggren, J. Phys. A **35**, L87 (2002).
[20] H. Ishio, A. I. Saichev, A. F. Sadreev, and K.-F. Berggren, Phys. Rev. E **64**, 056208 (2001).
[21] K. J. Ebeling, *Statistical Properties of Random Wave Fields in Physical Acoustics: Principles and Methods* (Academic Press, New York, 1984).
[22] A. F. Sadreev and K.-F. Berggren, Phys. Rev. E **70**, 026201 (2004).
[23] A. F. Sadreev, Phys. Rev. E **70**, 016208 (2004).